Available online at www.sciencedirect.com
ScienceDirect
Thin Solid Films 515 (2006) 1192–1196
www.elsevier.com/locate/tsf

Silicon–metal clusters: Nano-templates for cluster assembled materials

G.K. Gueorguiev [a,*], J.M. Pacheco [b], S. Stafström [a], L. Hultman [a]

[a] Department of Physics, Chemistry and Biology (IFM), Linköping University, S-581 83 Linköping, Sweden
[b] Centro de Física Teórica e Computacional and Departamento de Física da Faculdade de Ciências, Complexo Interdisciplinar da Universidade de Lisboa, Av. Prof. Gama Pinto 2, P-1649-003, Lisboa Codex, Portugal

Available online 7 September 2006

Abstract

The structure, cohesive energy and electronic properties of MSi_n clusters were studied by first-principles calculations as a function of size (n) and species (M). We investigated 168 different clusters, containing from 1 to 14 Si atoms together with one transition metal atom among 12 different elements: Ti, Zr, Hf, V, Nb, Ta, Ni, Pd, Pt, Cu, Ag, Au. Clusters with $n=7$, 10, 12 appear as local maxima in cohesive energy, independently of the metal involved. This, together with our previous findings for MSi_n (containing 12 other transition metal elements), establishes a systematic behavior. For most metals, MSi_{12} and MSi_{10} (the smallest endohedral species) are highly symmetric and exhibit local (with respect to their neighbors in size) stability. Thus, besides practically all MSi_{12} clusters (exceptions being $HfSi_{12}$, $ZrSi_{12}$), also some MSi_{10} such as VSi_{10}, $NiSi_{10}$, $PdSi_{10}$, $NbSi_{10}$ and $AgSi_{10}$, are promising candidates as building blocks for cluster assembled materials. Electronic properties of structurally equivalent clusters depend markedly on the transition metal involved, providing the means to tailor pre-defined properties when designing extended phases.

Keywords: Silicon clusters; First-principles calculations; Cluster-assembled materials; Transition metals

1. Introduction

The production of nanosized cluster-assembled materials is often based on the preparation of separated clusters which are made to condensate into a bulk-like material or to embed into a solid matrix. Condensed phases comprised of building blocks of silicon-transition metal MSi_n are expected to show novel properties, not attainable from the corresponding silicides and silicon–metal solid solutions. The latter already have multiple applications in the development of new devices for high-temperature electronics and as engineering materials for high-temperature coatings, integrated circuits, and special ceramics. The eventual synthesis of a material made of metal-containing silicon clusters would radically extend the present applications to new technological areas, e.g., the emerging area of nano-optoelectromechanical systems, as well as improve their quality in already established technologies.

The earliest experimental study of MSi_n clusters was conducted by Beck [1]. Later, theoretical calculations indicated the stability of $ZrSi_{20}$ [2], MSi_{15} [3], and MSi_{16} [4]. Recently, Hiura et al. [5] synthesized mixed silicon clusters, using as a nucleation site a single transition metal atom reacting with silane (SiH_4). The mass spectra of these MSi_n^{1+} species (M=Ta, W, Re, Ir) indicated that clusters with 12 silicon atoms and regular prismatic shape are abundant [5,6]. Theoretical studies by others showed similar geometries for $CrSi_{12}$ and $FeSi_{12}$ [7] as well as for $CuSi_{12}$, $MoSi_2$, and WSi_{12} [8].

In a recent work [9], we studied neutral MSi_n clusters by means of first-principles calculations within the framework of density functional theory (DFT) in its generalized gradient approximation (GGA). A total of 168 different MSi_n clusters, for which $1 \le n \le 14$ and "M" belongs to one of the 12 transition elements grouped into: [Cr, Mo, W], [Mn, Tc, Re], [Fe, Ru, Os], and [Co, Rh, Ir], were investigated. We found regularities in their structural behavior as well as in their electronic properties as a function of n, which may be explored in the design of cluster-based nanodevices. Clusters with $n=7$ and $n=12$ emerged as more stable than species with $n=6$, 8 and $n=11$, 13, respectively. The geometries of MSi_7 and MSi_{12} are–apart from minor distortions–independent of the transition metal species.

* Corresponding author. Tel.: +46 13 28 24 91; fax: +46 13 28 89 18.
E-mail address: gekos@ifm.liu.se (G.K. Gueorguiev).

0040-6090/$ - see front matter © 2006 Elsevier B.V. All rights reserved.
doi:10.1016/j.tsf.2006.07.114

In the present paper, investigating the same range between 1 and 14 Si atoms, we extend the MSi_n systematic study to other 12 transition metals—[Ti, Zr, Hf], [V, Nb, Ta], [Ni, Pd, Pt], and [Cu, Ag, Au]. It was confirmed that also for most of these metals, the clusters with $n=7$, 12 appear as local maxima in cohesive energy. For the present set of metals, some additional features emerged—MSi_7 are not always particularly stable and the symmetry of MSi_{12} is more strongly affected by Jahn-Teller distortions. Interestingly, some endohedral MSi_{10} are not only similar in shape to previously reported $FeSi_{10}$ and $CoSi_{10}$ [9], but rather stable. In agreement with our previous results [9] and as shown by others [10,11] the 18-electron rule (applicable for, e.g., WSi_{12} where each Si atom contributes one electron and the tungsten atom 6 electrons) is of limited applicability to MSi_n systems and cannot explain their relative stability and electronic properties.

As found for the set of metals we studied previously [9], the electronic properties of structurally equivalent clusters depend sensitively on the transition metal involved, providing the means to tailor specific properties when designing cluster-assembled materials (cf., however, Ref. [12], in which a simulation of MSi_{12} (M=Nb, W) solid phase showed that cage structure of the building blocks disappears during optimization).

In the present work, the layout of the results is deliberately the same as in [9]. Thus, comparisons through all 24 transition metal elements are promoted and a generalization of the MSi_n systematics is achieved.

2. Computational methods

All optimizations of MSi_n were carried out within the GGA-DFT, using both the ADF package [13] and the GAUSSIAN 03 program [14]. For comparative reasons, different basis sets (Slater-type, Gaussian) and different exchange-correlation functionals (PW91) [15] and the B3LYP hybrid functional [16] were used. Both PW91 and B3LYP are known to provide an accurate description of the structural and electronic properties of organometallic clusters [9,12,17–20]. Thus, we ensure that the reported trends in MSi_n systematics are independent on the calculation framework. The details of the optimization strategies (specifically improved to provide more reliable sampling of the potential energy hypersurface) are presented elsewhere [9]. The results reported here have been obtained by using PW91 and triple-zeta basis sets with polarization functions.

3. Results and discussion

3.1. Relative stability of MSi_n

Fig. 1 shows the cohesive energies divided by the number of silicon atoms (n), $|E_{coh}(n)|/n$, obtained for the energetically most favorable MSi_n structures. Maxima of the curves correspond to clusters displaying enhanced local stability. The curves in Fig. 1 allow comparisons both within each panel (one group of the Periodic Table), and across the four different panels (different groups). Considerable similarities for size dependence of $|E_{coh}(n)|/n$ both within each panel and across the panels are observed. These trends are even more pronounced for the lighter elements

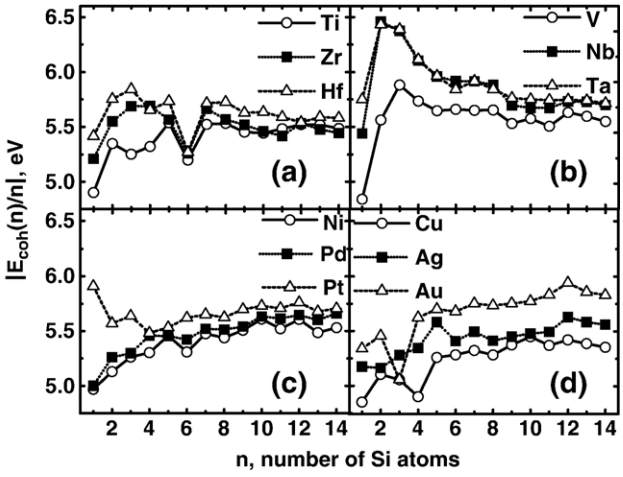

Fig. 1. Absolute value of the cohesive energy divided by the number of silicon atoms ($|E_{coh}(n)|/n$) as a function of size (n) and species M for different MSi_n clusters. Each data point corresponds to the equilibrium geometry of a given MSi_n cluster. Panels (a)–(d) correspond to groups IV-B, V-B, X-B and XI-B of the Periodic Table. Within each panel the clusters for which the transition metal element has smallest atomic number Z are drawn with a solid line and open circles, those with intermediate value of Z with a dotted line and solid squares, and the largest atomic number corresponds to the dashed line and open triangles.

such as Ti, Zr, V, Nb, Pd, whereas Hf and Ta show irregularities with respect to that behavior. Overall, $|E_{coh}(n)|/n$ has a minimum for $n=6$, after which $n=7$ emerges as a local maximum (generally less pronounced than for the MSi_n studied in [9]). The local maxima for $n=12$ are again well defined. In contrast to Ref. [9], the maxima within one panel in Fig. 1 vary more: whereas for Ni, V and Au the local stability of MSi_{12} is even higher than that reported for most metals (e.g., Cr, Ir, Os) in [9], $HfSi_{12}$ and $TaSi_{12}$ are not a local maximum at all.

The features of size evolution are better viewed by plotting the second difference spectra $\Delta(n)$

$$\Delta(n) = |E_{coh}(n+1) + E_{coh}(n-1) - 2E_{coh}(n)|/2, \quad (1)$$

where $2 \le n \le 13$. The size and species dependence of $\Delta(n)$ are shown in Fig. 2, using the same notation as in Fig. 1. The differential character of $\Delta(n)$ leads to sharpened extrema thus exposing better the less well defined extrema, e.g., at $n=5$. In Fig. 2, one can see another general trend (also present in Ref. [9]): for most of the transition metal elements, maxima occur for odd n values when $n<10$, and for even values of n when $n \ge 10$. This feature of the size dependence of E_{coh} correlates with the finding that the smallest cluster size for which an endohedral equilibrium shape emerges corresponds to species with $n=10$ Si atoms. New features with respect to [9] are the following:

(i) The maxima at $n=5$, 7 are frequently less pronounced (V, Nb, Pt);
(ii) The maxima corresponding to MSi_{10} clusters are better defined (V, Ni, Pd, Cu, Ag).

The MSi_{12} and to a lesser extent MSi_7 were discussed as key species in [9]. For the metals belonging to the "outer" groups

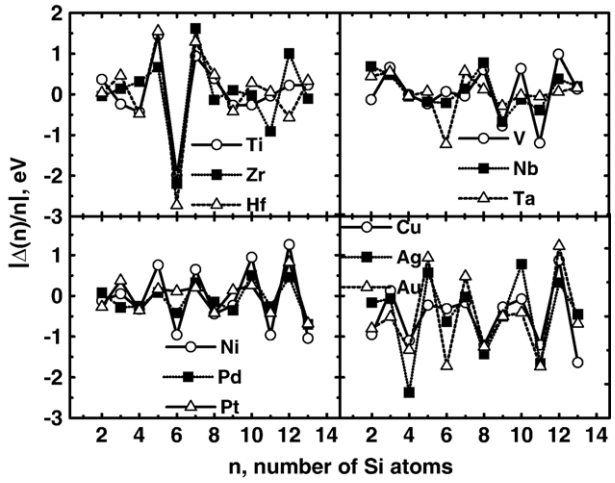

Fig. 2. The second difference spectra of cohesive energy $\Delta(n)$ plotted as a function of n for $2 \le n \le 13$.

of the Periodic Table (IV-B, V-B—early transition metals, and X-B, XI-B—late transition metals), along with the preserved stability of MSi_{12}, the MSi_{10} emerge as a class of clusters with markedly enhanced local stability. Overall, the open MSi_7 structures do not exhibit so distinguished maxima in E_{coh} as they do for the "inner" submatrix of transition metal elements.

3.2. Equilibrium shapes of MSi_n

The MSi_3 clusters (usually locally stable) exhibit the shape of a pyramid shown in Fig. 3a. Alternative planar rhombic shape (Fig. 3a, inset) found in [9] for Rh, Ru, Co, Fe was not observed for the presently studied metals.

The capped trapezoid form shown in Fig. 3b, typical for clusters with MSi_5 in [9], is preserved also for all the elements studied here, but for Ni. For $NiSi_5$, the trapezoid becomes a square (Fig. 3b, inset) as previously found for $CoSi_5$ and $RhSi_5$.

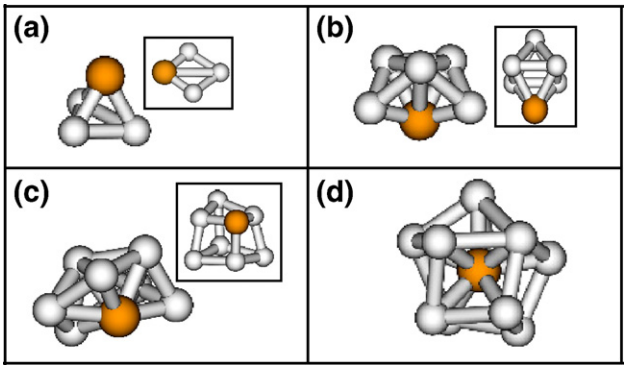

Fig. 3. Typical equilibrium shapes of MSi_n ($n<12$) clusters. In the insets equilibrium structures for minority of metal elements (where such alternatives were detected): (a) the triangular pyramid shape typical for clusters with $n=3$ (inset: the planar rhombic shape, see main text); (b) the capped trapezoid form typical for $n=5$ (inset: the capped square bipyramid found for $NiSi_5$); (c) the common shape for $n=7$ (inset: deformed cubic shape of $TaSi_7$, and $PtSi_7$); (d) the endohedral bicapped tetragonal antiprism (D_{4d}) of MSi_{10} (M=Ti, Hf, V, Nb, Ni, Pd, Cu, Ag, and Au).

Most MSi_7 clusters (Fig. 3c) share a common shape which does not belong to any special group of symmetry. However, $TaSi_7$ and $PtSi_7$ (Fig. 3c, inset) differ substantially and resemble a deformed cube.

For most MSi_n equilibrium structures with $n<12$, the metal atom is positioned at the edge of the cluster. However, in [9] two exceptions to this condition were found—$FeSi_{10}$ and $CoSi_{10}$. Exhibiting the endohedral structure shown in Fig. 3d, they were not particularly stable. Now, the endohedral structure displayed in Fig. 3d is confirmed as equilibrium shape for nine more metals—Ti, Hf, V, Nb, Ni, Pd, Cu, Ag and Au. The only differences between these MSi_{10} clusters comprise in slightly different bond lengths. In contrast, the remaining three species–$ZrSi_{10}$, $TaSi_{10}$ and $PtSi_{10}$–are not endohedral and not particularly symmetric. The conformation in Fig. 3d is a bicapped tetragonal antiprism revealing D_{4d} symmetry. However, small distortions (not exceeding 6% of the bond lengths needed for an ideal D_{4d} shape) prevent the MSi_{10} structures from being perfectly symmetric. Most of these nine endohedral clusters are locally stable and VSi_{10}, $NiSi_{10}$, $PdSi_{10}$, and $AgSi_{10}$ are not only rather stable, but also the most symmetric. To be noted, that after the first discussion of endohedral MSi_{10} in [9], Neukermans et al. reported experimental and theoretical evidence for marked stability of an endohedral bicapped tetragonal antiprism (D_{4d}) with stoichiometry $AlPb_{10}$ [21]. These results enhance the hopes that also the MSi_{10}'s are synthesizable. Therefore, future theoretical studies of condensed phases based on MSi_{12} and experimental attempts for depositing MSi_{12} films should take into account a possible presence of MSi_{10} in the gas phase and eventual competition between MSi_{12} and MSi_{10} during the deposition process.

For MSi_{12}, the local stability of the hexagonal prism with D_{6h} symmetry, depicted in Fig. 4a, is not surprising [5–7,11,12,17]. Distortions from the two perfectly aligned Si-hexagons were observed for most of the metals considered here, except for Nb, Ta, and Pd for which MSi_{12} are perfect hexagonal cages. Again, there is a difference between the "inner" [9] and the "outer" groups of transition metal elements. Whereas in [9] such distortions (not exceeding 5% of the bond lengths corresponding to a perfect D_{6h} shape) were detected for 5 transition metal elements (Co, Fe, Tc, Ru, and Os), most of the metals belonging to the

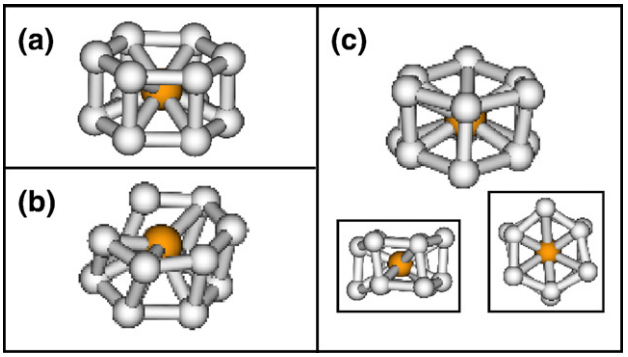

Fig. 4. Different variants of the prismatic shape of MSi_{12}: (a) the perfect (D_{6h}) form of $NbSi_{12}$, $TaSi_{12}$ and $PdSi_{12}$; (b) the strongly distorted $ZrSi_{12}$; (c) the specific Jahn-Teller distortion of the prism shared by $TiSi_{12}$, $NiSi_{12}$, VSi_{12}, and $PtSi_{12}$ with its side and top views (insets).

"outer" groups exhibit distortions and these distortions are larger (5–9% deviation from the bond lengths of an ideal D_{6h}), $ZrSi_{12}$ being the most distorted one. Fig. 4a and b show the perfectly symmetric $NbSi_{12}$, and the most distorted cluster, $ZrSi_{12}$, respectively. The deformed but still sandwich-like structure of $ZrSi_{12}$ is in agreement with recent DFT results by Wang and Han [19]. They found that for $ZrSi_{12}$ the D_{6h} shape is strongly deformed as compared to other MSi_{12}, and that the Zr atom may even migrate to the cluster surface. We found that, similarly to $ZrSi_{12}$, also $HfSi_{12}$ is strongly distorted. Thus, from all 24 transition metal elements studied by us ([9] and this work), $HfSi_{12}$ and $TaSi_{12}$ are the only cases of MSi_{12} lacking a local stability.

For $TiSi_{12}$, $NiSi_{12}$, VSi_{12}, and $PtSi_{12}$ (Fig. 4c), we found a distortion consisting of an imperfect perpendicularity of the cluster vertices to the hexagonal planes. Typical for all distorted MSi_{12} clusters is that the distortions within the hexagons are larger (2.1%–5.5%) than any distortions perpendicular to the hexagonal planes (0.8%–1.3%). Although relatively small, such distortions should be taken into account when considering packing rules for extended phases. In contrast, cluster distortions strongly depending on the involved metal would be unfavorable for packing clusters with different M.

The $MSi_{10,12}$ distortions are due to the Jahn-Teller effect which is widely discussed in other mixed clusters such as the met-cars [22,23]. The epikernel principle requires that Jahn-Teller distortions preserve as many symmetry elements as possible. This is in agreement with the conformation shown in Fig. 4c and the insets in it which lost the ideal D_{6h} symmetry but still preserves some symmetry (the configurational instability of certain MSi_{12} is removed by symmetry lowering).

According to the 18-electron rule the most stable MSi_{12}'s should be $CrSi_{12}$, $MoSi_{12}$, and WSi_{12}, whereas the most stable MSi_{10}'s should be $FeSi_{10}$, $RuSi_{10}$, and $OsSi_{10}$. However, the results shown in Figs. 1 and 2 together with those in [9] indicate that in the case of MSi_{12}, there are many more (besides Cr, Mo, W) stable MSi_{12}'s in which the metal atom has $N \neq 6$ valence electrons ($TcSi_{12}$ and $RhSi_{12}$ are even more stable than WSi_{12} and $MoSi_{12}$). For $n=10$, $FeSi_{10}$ is not locally stable at all; $RuSi_{10}$ and $OsSi_{10}$ are not locally stable and not cage-like, whereas $TiSi_{10}$, VSi_{10}, and $PdSi_{10}$ are locally stable, symmetric and cage-like. A possible explanation of the limited applicability of the 18-electron rule is that the structure and stability of MSi_n is determined by an interplay between geometric (related to close-packing, such as size of the metal atom, distribution of the dangling bonds of silicon), and electronic (closed-shell) factors.

3.3. Electronic properties of MSi_n

For single clusters, the HOMO-LUMO gap (the difference between the highest occupied molecular orbital and the lowest unoccupied molecular orbital) is a prototypic electronic property with an impact on the stability of corresponding solid phase. Fig. 5 displays the evolution of the HOMO-LUMO gaps as a function of n, using the same style as in Fig. 1. Since the main part of the optimization work on MSi_n has been carried out within spin-unpolarized GGA, only the clusters containing Ti, Zr, Hf, Ni, Pd and Pt have finite HOMO-LUMO gaps. Extensive tests to check the implication of the spin effects have been performed in a similar way as in Ref. [9]. Again, it was concluded that the spin effects do not play a significant role in the characterization of the properties of relevance for this systematics. We believe that this is a result of the fact that each cluster contains only one transition metal atom. The data in Fig. 5 show that the clusters with $n=10$ and $n=12$ exhibit a wide range of HOMO-LUMO gaps (0.6 eV–1.3 eV for MSi_{12}, and 0.7–1.6 eV for MSi_{10}) for the different metal elements. A similar variation applies also to the stable, but non-endohedral MSi_5 and MSi_7. When compared to pure Si clusters, the MSi_n due to the transition metal atom M exhibit smaller HOMO-LUMO gaps and do not follow the size dependence known for Si nano-structures [24]. Generally, the underlying organization of the Periodic Table defines the behavior of the HOMO-LUMO gaps—elements of the same group display similar HOMO-LUMO gaps. However, Ni behaves differently and is "out of phase" with respect to the other elements in its group (see Fig. 5). In a similar way in [9], another light metal in its group with magnetic properties, Fe, represents an exception concerning the variations in the HOMO-LUMO gap size dependence.

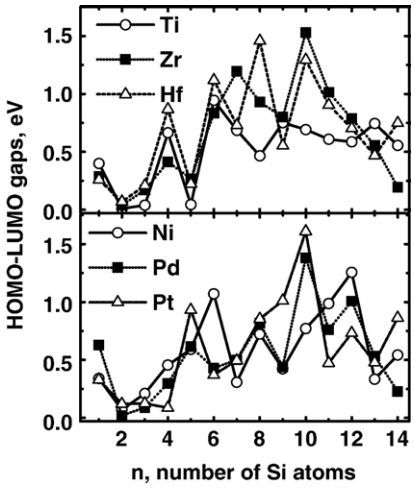

Fig. 5. Size evolution of the HOMO-LUMO gaps of MSi_n as a function of M and n. The upper panel corresponds to the elements of panel (a) in Fig. 1 and the bottom panel to those elements of panel (c) in Fig. 1.

The static polarizability of isolated clusters is related to their optical properties and can be viewed as complementary information to their geometry and bonding nature. We calculated the static polarizabilities (α_{xx}, α_{yy}, α_{zz}) along the principal axes for all MSi_{12} clusters and for those of MSi_{10} which are endohedral. The average polarizabilities $\langle\alpha\rangle$ were calculated according to the formula:

$$\langle\alpha\rangle = \frac{1}{3}\left(\alpha_{xx} + \alpha_{yy} + \alpha_{zz}\right). \quad (2)$$

The directional polarizabilities α_{ii} (where $i=x, y, z$ are the principal axes of the clusters) directly reflect the shape and the size of the clusters, including the small Jahn-Teller distortions (where present). The average polarizabilities for MSi_{12} vary

between 54.5 Å^3 ($CuSi_{12}$) and 61.1 Å^3 ($HfSi_{12}$). The MSi_{12} containing a metal from the IV-B group of the Periodic Table (with largest atomic radii within the studied transition metals) display the largest polarizabilities. By changing the transition metal atom within the same group of the Periodic Table, the variation of the average polarizability does not exceed 3.3%. Heavier atoms are larger in size and correspond to MSi_n with increased volume and correspondingly increased average polarizability. Considering all 12 metals studied here, the maximum variation of $\langle\alpha\rangle$ reaches 10.8%. The endohedral MSi_{10} clusters, due to their D_{4d} group of symmetry, display lower differences between their directional polarizabilities than MSi_{12}. The MSi_{10} average static polarizabilities (e.g., 49.6 Å^3 for $CuSi_{10}$) follow closely those of their MSi_{12} counterparts, however, at an approximately 8–10% lower level due to the smaller volume of MSi_{10}.

4. Conclusions

Making use of first-principles GGA-DFT simulations, we have extended the study of the equilibrium shapes, stability and electronic properties of MSi_n ($1 \le n \le 14$) clusters adding 12 new transition metal elements, [Ti, Zr, Hf], [V, Nb, Ta], [Ni, Pd, Pt] and [Cu, Ag, Au], to the 12 previously studied. The emphasis was put on general trends, similarities, and features relevant for the synthesis of cluster-assembled materials. Clusters with $n=12$ exhibit an enhanced local stability with an emblematic hexagonal prism (D_{6h}) equilibrium structure for all the transition metals. For the MSi_{10} clusters, the bicapped tetragonal antiprism (D_{4d}) is predominant. Irrespective of the striking structural similarities found for those cage-like templates with the same number of Si atoms, paradigmatic (representative) properties such as HOMO-LUMO gap and static polarizability, exhibit species dependences which qualitatively reflect the organization (by group: valency and by period: atomic size) of the transition metals in the Periodic Table. A new aspect added to the understanding of MSi_n is that for most of transition metals belonging to the IV-B, V-B, X-B, and XI-B groups the MSi_{10} cages deserve consideration as an important alternative to MSi_{12} in future attempts for synthesis of MSi_n clusters and their subsequent self-assembly into extended phases. While most of the considered metals are promising candidates for synthesizing MSi_{12} clusters, the most prospective elements for MSi_{10} are Ni, Pd, V, Nb, and Ag. Finally, we conclude that the combination of structural similarities with diversity in electronic properties for the MSi_n clusters makes them potentially useful as building blocks (nano-templates) for the synthesis of extended phases.

Acknowledgements

The research was supported by The Swedish Foundation for Strategic Research (SSF), Strategic Research Centre on Materials Science for Nanoscale Surface Engineering (MS^2E) and the European Commission. The National Supercomputer Center in Linköping is gratefully acknowledged for providing high performance computing resources. J.M.P. acknowledges financial support from The Portuguese Foundation for Science and Technology under Project POCI/FP/58418/2004.

References

[1] S.M. Beck, Adv. Metal Semicond. Clust. 1 (1993) 241.
[2] K. Jackson, B. Nellermoe, Chem. Phys. Lett. 254 (1996) 249.
[3] J.G. Han, Y.Y. Shi, Chem. Phys. 266 (2001) 33.
[4] V. Kumar, Y. Kawazoe, Phys. Rev. Lett. 87 (2001) 045503.
[5] H. Hiura, T. Miyazaki, T. Kanayama, Phys. Rev. Lett. 86 (2001) 1733.
[6] T. Miyazaki, H. Hiura, T. Kanayama, Phys. Rev., B 66 (2002) 121403.
[7] S.N. Khanna, B.K. Rao, P. Jena, S.K. Nayak, Chem. Phys. Lett. 373 (2003) 433.
[8] F. Hagelberg, C.Y. Xiao, W.A. Lester Jr., Phys. Rev., B 67 (2003) 035426.
[9] G.K. Gueorguiev, J.M. Pacheco, J. Chem. Phys. 119 (2003) 10313.
[10] P. Sen, L. Mitas, Phys. Rev., B 68 (2003) 155404.
[11] W. Zheng, J.M. Nilles, D. Radisic, K.H. Bowen Jr., J. Chem. Phys. 122 (2005) 071101.
[12] J.M. Pacheco, G.K. Gueorguiev, J.L. Martins, Phys. Rev. B66 (2002) 033401.
[13] G. te Velde, E.J. Baerends, J. Comp. Phys. 99 (1992) 84.
[14] M.J., Frisch, Gaussian, Inc., Wallingford, CT (2003).
[15] J.P. Perdew, J.A. Chevary, S.H. Vosko, K.A. Jackson, M.R. Pederson, D.J. Singh, C. Fiolhais, Phys. Rev., B 46 (1992) 6671.
[16] A.D. Becke, J. Chem. Phys. 98 (1993) 5648.
[17] P. Guo, Z.-Y. Ren, F. Wang, J. Bian, J.-G. Han, G.-H. Wang, J. Chem. Phys. 121 (2004) 12265.
[18] H. Kawamura, V. Kumar, Y. Kawazoe, Phys. Rev., B 71 (2005) 075423.
[19] J. Wang, J.-G. Han, J. Chem. Phys. 123 (2005) 064306.
[20] G.K. Gueorguiev, J.M. Pacheco, Phys. Rev. Lett. 88 (2002) 115504.
[21] S. Neukermans, E. Janssens, Z.F. Chen, R.E. Silverans, P.v.R. Schleyer, P. Lievens, Phys. Rev. Lett. 92 (2004) 163401.
[22] A. Ceulemans, P.W. Fowler, J. Chem. Soc., Faraday Trans. 88 (1992) 2797.
[23] M.-M. Rohmer, M. Bénard, J.-M. Poblet, Chem. Rev. 100 (2000) 495.
[24] B. Delley, E.F. Steigmeier, Appl. Phys. Lett. 67 (1995) 2370.